STRUCTURAL BIOLOGY COMMUNICATIONS

ISSN 2053-230X

The crystal structure of human DEAH-box RNA helicase 15 reveals a domain organization of the mammalian DEAH/RHA family

Karin Murakami,[a]‡ Kenji Nakano,[a]‡ Toshiyuki Shimizu[a,b]* and Umeharu Ohto[a]*

[a]Graduate School of Pharmaceutical Sciences, The University of Tokyo, 7-3-1 Hongo, Bunkyo-ku, Tokyo 113-0033, Japan, and [b]Core Research for Evolutional Science and Technology (CREST), Japan Science and Technology Agency (JST), Saitama 332-0012, Japan. *Correspondence e-mail: shimizu@mol.f.u-tokyo.ac.jp, umeji@mol.f.u-tokyo.ac.jp

Received 31 March 2017
Accepted 17 May 2017

Edited by I. Tanaka, Hokkaido University, Japan

‡ These authors contributed equally to this work.

Keywords: RNA helicase 15; DEAH-box; DEAH/RHA family; innate immunity; DHX15.

PDB reference: DHX15, 5xdr

Supporting information: this article has supporting information at journals.iucr.org/f

DEAH-box RNA helicase 15 (DHX15) plays important roles in RNA metabolism, including in splicing and in ribosome biogenesis. In addition, mammalian DHX15 also mediates the innate immune sensing of viral RNA. However, structural information on this protein is not available, although the structure of the fungal orthologue of this protein, Prp43, has been elucidated. Here, the crystal structure of the ADP-bound form of human DHX15 is reported at a resolution of 2.0 Å. This is the first structure to be revealed of a member of the mammalian DEAH-box RNA helicase (DEAH/RHA) family in a nearly complete form, including the catalytic core consisting of the two N-terminal RecA domains and the C-terminal regulatory domains (CTD). The ADP-bound form of DHX15 displayed a compact structure, in which the RecA domains made extensive contacts with the CTD. Notably, a potential RNA-binding site was found on the surface of a RecA domain with positive electrostatic potential. Almost all structural features were conserved between the fungal Prp43 and the human DHX15, suggesting that they share a fundamentally common mechanism of action and providing a better understanding of the specific mammalian functions of DHX15.

1. Introduction

Helicases are nucleic acid-dependent nucleoside triphosphatases (NTPases) that are involved in many biological processes associated with nucleic acid metabolism, such as transcription, translation, splicing and remodelling of ribonucleoprotein complexes (Singleton *et al.*, 2007). These proteins have been classified into six superfamilies (SF1–SF6) based on their sequence, structure and function (Singleton *et al.*, 2007). SF1 and SF2 helicases possess a conserved catalytic core consisting of two RecA-like domains (RecA1 and RecA2) with sequence motifs (I, Ia, Ib, II, III, IV, V and VI) for helicase functions such as ligand binding or NTP hydrolysis (Fairman-Williams *et al.*, 2010; Abdelhaleem *et al.*, 2003). SF2 contains the largest number of proteins and is further classified into ten subfamilies with different N-terminal and C-terminal domains with divergent functions; for example, DEAD-box, RIG-I-like, Ski2-like and DEAH/RHA families (Fairman-Williams *et al.*, 2010). The DEAH/RHA family is named after the DEAH (Asp-Glu-Ala-His) box (motif II) sequence and RNA helicase (RHA) A (DHX9), and is characterized by six structural regions: the N-terminal extension, the RecA1 and RecA2 domains, the winged-helix (WH) domain, the ratchet domain and the oligonucleotide/oligosaccharide-binding (OB)-fold domain (Fig. 1). The

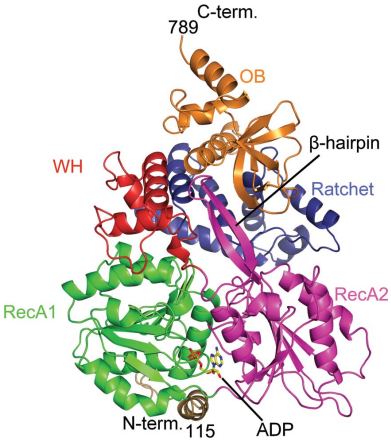

N-terminal extension is not conserved among members of the DEAH/RHA family, while the three C-terminal domains (CTD) are well conserved.

DEAH-box RNA helicase 15 (DHX15) is a member of the DEAH/RHA family. It plays important roles in RNA metabolism, including in splicing and ribosome biogenesis (Abdelhaleem *et al.*, 2003; Imamura *et al.*, 1997). The helicase activity of DHX15 is required for disassembling the spliceosome, modulating the splicing of pre-messenger RNAs and processing the early stages of pre-ribosomal RNA splicing, and is regulated by interaction with a number of proteins containing a G-patch domain (Robert-Paganin *et al.*, 2015), such as tuftelin-interacting protein 11 (TFIP11; Tannukit *et al.*, 2009), RNA-binding protein 5 (RBM5; Niu *et al.*, 2012) and

Figure 1
Sequence alignment between DHX15 and Prp43. A sequence alignment of DHX15 from human (DHX15_HUMAN), mouse (DHX15_MOUSE) and *Drosophila melanogaster* (DHX15_DROME) and of Prp43 from *Saccharomyces cerevisiae* (PRP43_YEAST) and *Chaetomium thermophilum* (PRP43_CHATD) is shown. The sequences were derived from UniProt (http://www.uniprot.org/) and were aligned using *CLUSTALW* (http://www.genome.jp/tools/clustalw/). The figure was prepared using *ESPript*3 (http://espript.ibcp.fr/ESPript/cgi-bin/ESPript.cgi; Robert & Gouet, 2014). The secondary structure of human DHX15 is shown at the top of each block. The residues involved in the interaction with ssRNA in ctPrp43 (Tauchert *et al.*, 2017) are highlighted with black stars.

Table 1
Macromolecule information for DHX15.

Additional residues after the cleavage of the 6×His tag and FLAG tag with PreScission protease are underlined.

Source organism	*Homo sapiens*
DNA source	cDNA
Expression vector	pFastBac Dual
Expression host	Sf9 cells
Complete amino-acid sequence of the construct	GPEFSLPQCINPFTNLPHTPRYYDILKKRLQLPV-WEYKDRFTDILVRHQSFVLVGETGSGKTTQIP-QWCVEYMRSLPGPKRGVACTQPRRVAAMSVAQ-RVADEMDVMLGQEVGYSIRFEDCSSAKTILKY-MTDGMLLREAMNDPLLERYGVIILDEAHERTL-ATDILMGVLKEVVRQRSDLKVIVMSATLDAGK-FQIYFDNCPLLTIPGRTHPVEIFYTPEPERDY-LEAAIRTVIQIHMCEEEEGDLLLFLTGQEEID-EACKRIKREVDDLGPEVGDIKIIPLYSTLPPQ-QQQRIFEPPPPKKQNGAIGRKVVVSTNIAETS-LTIDGVVFVIDPGFAKQKVYNPRIRVESLLVT-AISKASAQQRAGRAGRTRPGKCFRLYTEKAYK-TEMQDNTYPEILRSNLGSVVLQLKKLGIDDLV-HFDFMDPPAPETLMRALELLNYLAALNDDGDL-TELGSMMAEFPLDPQLAKMVIASCDYNCSNEV-LSITAMLSVPQCFVRPTEAKKAADEAKMRFAH-IDGDHLTLLNVYHAFKQNHESVQWCYDNFINY-RSLMSADNVRQQLSRIMDRFNLPRRSSDFTSR-DYYINIRKALVTGYFMQVAHLERTGHYLTVKD-NQVVQLHPSTVLDHKPEWVLYNEFVLTTKNYI-RTCTDIKPEWLVKIAPQYYDMSNFPQCEAKRQ-LDRIIAKLQSKEYSQY
Formula weight of entity (Da)	79014.9

NF-κB-repressing factor (NKRF; Memet *et al.*, 2017). Apart from being involved in RNA metabolism, DHX15 also mediates antiviral innate immune responses. DHX15, along with NLRP6 (NLR family, pyrin domain-containing 6), recognizes viral RNA and stimulates mitochondrial antiviral signalling (MAVS) proteins to induce type I/III interferons during viral infection (Wang *et al.*, 2015). Other members of SF2 have also been shown to be involved in antiviral innate immunity, including RIG-I, MDA5, DDX1, DDX3, DHX9, DDX21 and DHX33 (Liu *et al.*, 2014; Mitoma *et al.*, 2013; Zhang, Yuan *et al.*, 2011; Zhang, Kim *et al.*, 2011; Miyashita *et al.*, 2011; Oshiumi *et al.*, 2010; Myong *et al.*, 2009).

Although very little has been reported about the mechanism of action of mammalian DHX15, Prp43, a fungal orthologue of DHX15, has been studied in some detail, including its structural information. Prp43 and DHX15 have overlapping functions in RNA splicing and ribosome biogenesis, which are regulated by G-patch-containing proteins (Fourmann *et al.*, 2013; Tanaka & Schwer, 2006; Leeds *et al.*, 2006; Combs *et al.*, 2006; Lebaron *et al.*, 2005, 2009; Bohnsack *et al.*, 2009; Chen *et al.*, 2014; Pertschy *et al.*, 2009); however, participation in innate immunity has only been reported for mammalian DHX15 (Wang *et al.*, 2015; Lu *et al.*, 2014). Crystal structures of Prp43 from *Saccharomyces cerevisiae* (scPrp43) and *Chaetomium thermophilum* (ctPrp43) have revealed its overall architecture and RNA-recognition mechanism (Tauchert *et al.*, 2016, 2017; Walbott *et al.*, 2010; He *et al.*, 2010); these studies have shown that Prp43 shares structural homology with the Ski2-like DNA helicase Hel308 (Walbott *et al.*, 2010; Büttner *et al.*, 2007). The CTD (WH, ratchet and OB-fold domains) is located on the RNA-binding surface of the two RecA domains and has been suggested to act as a regulatory domain for RNA binding, thus coupling ATP hydrolysis to RNA unwinding, and interaction with G-patch-containing proteins using the OB-fold domain.

Currently, structural information on mammalian DEAH/RHA proteins is only available for the CTD of human DHX8 (Kudlinzki *et al.*, 2012) and part of the N-terminal extension of human DHX9 (Fu & Yuan, 2013). In this study, we describe the crystal structure of human DHX15 in complex with ADP. This is the first structure to be revealed of a mammalian DEAH/RHA protein and contains the catalytic core consisting of two RecA domains and the regulatory CTD. We identified a potential RNA-binding site at a pocket with high positive electrostatic potential between the RecA domains and the CTD. Almost all structural elements were conserved between the fungal Prp43 and the human DHX15. This suggests that the fundamental mechanism of action might be conserved. It also provides clues to understanding the specific mammalian functions of DHX15.

2. Materials and methods

2.1. Macromolecule production

The gene encoding DHX15 (residues 110–795) with a point mutation (S678T) was amplified from the genomic cDNA library of *Homo sapiens* and inserted downstream of a 6×His tag, a FLAG tag and a PreScission Protease cleavage site in a modified pFastBac Dual expression vector (Thermo Fisher Scientific). The recombinant DHX15 was expressed in Sf9 cells at 300 K for 70 h after infection. The cells were collected and lysed by sonication. After centrifugation at 20 000 rev min^{-1}, the protein was purified from the cleared lysate using Ni–NTA resin (Qiagen). The protein was treated with PreScission protease to cleave the purification tags and was then purified using a Superdex 200 gel-filtration column (GE Healthcare). The protein was concentrated to 24.7 mg ml^{-1} in crystallization buffer consisting of 25 m*M* Tris–HCl pH 8.0, 500 m*M* NaCl, 10% glycerol, 5 m*M* $MgCl_2$, 1 m*M* ADP, 1 m*M* DTT. Information regarding macromolecule production is summarized in Table 1.

2.2. Crystallization, data collection and structure determination

Crystals of DHX15 were grown at 293 K by mixing the protein solution with an equal volume of reservoir solution [0.18 *M* lithium sulfate, 0.09 *M* sodium acetate, 0.09 *M* HEPES–NaOH pH 7.5, 22.5%(*w*/*v*) PEG 4000] using the sitting-drop vapour-diffusion method. Crystallization information is summarized in Table 2.

The crystals were equilibrated in a cryoprotectant solution consisting of the reservoir solution supplemented with 350 m*M* NaCl and 20% ethylene glycol. X-ray diffraction data were collected (λ = 1.0000 Å) on beamline NE3A at the Photon Factory Advanced Ring (PF-AR), Ibaraki, Japan under cryogenic conditions at 100 K. The X-ray diffraction

Table 2
Crystallization.

Method	Sitting-drop vapour diffusion
Plate type	CrystalClear P Strip without indent, 96 wells per frame (Hampton Research)
Temperature (K)	293
Protein concentration (mg ml^{-1})	24.7
Buffer composition of protein solution	25 m*M* Tris–HCl pH 8.0, 500 m*M* NaCl, 10%(*v*/*v*) glycerol, 1 m*M* DTT, 5 m*M* $MgCl_2$, 1 m*M* ADP
Composition of reservoir solution	0.18 *M* lithium sulfate, 0.09 *M* sodium acetate, 0.09 *M* HEPES–NaOH pH 7.5, 22.5%(*w*/*v*) PEG 4000
Volume and ratio of drop	500 nl protein solution, 500 nl reservoir solution
Volume of reservoir (µl)	50

data were processed using *XDS* (Kabsch, 2010). The data-collection and processing statistics are summarized in Table 3.

The crystal structure of DHX15 was solved by molecular replacement with *MOLREP* (Vagin & Teplyakov, 2010), using the ADP-bound form of the yeast Prp43 structure (PDB entry 2xau; Walbott *et al.*, 2010) as a search model. The model was subjected to iterative cycles of manual model building using *Coot* (Emsley *et al.*, 2010) and restrained refinement using *REFMAC* (Murshudov *et al.*, 2011) (Table 4). The quality of the refined model was evaluated using *MolProbity* (Chen *et al.*, 2010). The structural figures were prepared with *PyMOL* (DeLano, 2008) or *CueMol* (http://www.cuemol.org). The coordinate and structure-factor data of DHX15 have been deposited in the Protein Data Bank (PDB) as entry 5xdr.

Table 3
Data-collection and processing statistics for DHX15.

Values in parentheses are for the outer shell.

Diffraction source	NE3A, PF-AR
Wavelength (Å)	1.0000
Temperature (K)	100
Detector	PILATUS 2M-F
Crystal-to-detector distance (mm)	242.8
Rotation range per image (°)	0.25
Total rotation range (°)	360
Exposure time per image (s)	0.25
Space group	$C222_1$
a, *b*, *c* (Å)	81.9, 89.4, 211.1
Matthews coefficient V_M (Å^3 Da^{-1})	2.13
Mosaicity (°)	0.15
Resolution range (Å)	45.83–2.00 (2.05–2.00)
Total No. of reflections	694119 (51328)
No. of unique reflections	52747 (3868)
Completeness (%)	100.0 (100.0)
Multiplicity	13.2 (13.3)
$\langle I/\sigma(I)\rangle$	16.5 (2.1)
R_{meas}†	0.083 (1.140)
Overall *B* factor from Wilson plot (Å^2)	38.2

† $R_{meas} = \sum_{hkl}\{N(hkl)/[N(hkl)-1]\}^{1/2}\sum_i |I_i(hkl) - \langle I(hkl)\rangle|/\sum_{hkl}\sum_i I_i(hkl)$ calculated for all data.

3. Results

3.1. Overall structure of human DHX15

We used a truncated mutant of human DHX15 (residues 110–795) for crystallization because the N-terminal extension was susceptible to cleavage (Table 1). We determined the

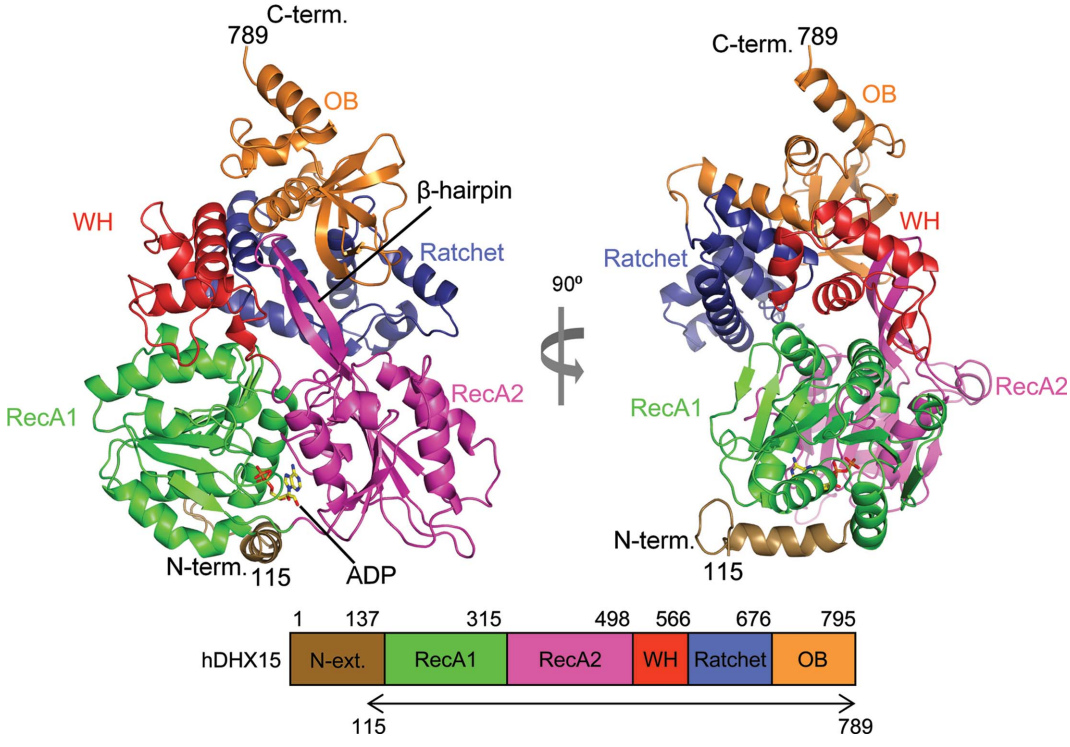

Figure 2
Overall structure of the ADP-bound form of DHX15. The ADP molecule is recognized by two RecA domains with a typical arrangement that is conserved in the helicase family. The front view (left) and side view (right) are shown. Each domain is coloured: the N-terminal extension in brown, the RecA1 domain in light green, the RecA2 domain in magenta, the WH domain in red, the ratchet domain in violet and the OB-fold domain in orange. The double-headed arrow at the bottom indicates the region contained in the final model.

crystal structure of human DHX15 in the ADP-bound form at a resolution of 2.0 Å (Tables 2, 3 and 4). The final model contained DHX15 residues 115–789, an ADP molecule, a magnesium ion, two sulfate ions and 82 water molecules; it was refined to R_{cryst} and R_{free} values of 22.8 and 26.5%, respectively (Table 4).

DHX15 has dimensions of about 60 × 80 × 40 Å and was divided into six domains (Tauchert *et al.*, 2016, 2017; Walbott *et al.*, 2010; He *et al.*, 2010; Fig. 2); the N-terminal extension (residues 1–137), the RecA1 (residues 138–315) and RecA2 (residues 316–498) domains, the WH domain (residues 499–566), the ratchet domain (residues 567–676) and the OB-fold domain (residues 677–795).

The two RecA domains of DHX15 made intimate contact with each other. This contact was mediated by ADP molecules and showed a typical arrangement that is conserved in the helicase family (Fairman-Williams *et al.*, 2010; Fig. 2). The CTD was located opposite the ADP-binding site in the RecA domains and made extensive contacts with both of the RecA domains. Of note, the protruding β-hairpin region of RecA2 domain was inserted into the space between the OB-fold and WH domains. The areas of contact between RecA1 and RecA2, between RecA1 and the CTD, and between RecA1 and the CTD were 836, 1082 and 850 Å^2, respectively. As a result, DHX15 folded into a compact structure.

3.2. DHX15 RecA domains have conserved nucleotide-binding motifs

DHX15 belongs to the SF2 helicases and possesses conserved sequence motifs, namely motifs I (^{160}GETGSGKTTQ^{169}), Ia (^{193}PRRVAA^{198}), Ib (^{237}TDGML^{241}), II (^{260}DEAH^{263}), III (^{292}SAT^{294}), IV (^{353}LLFLTGQE^{360}), V (^{421}TNIAETSLTIDGV^{433}) and VI (^{468}QRAGRAGR^{475}) (Abdelhaleem *et al.*, 2003; Tauchert *et al.*, 2016; Fig. 1). In the structure of ADP-bound DHX15, these motifs were arranged in a manner typical of DEAH/RHA proteins (Figs. 3*a* and 3*b*).

Table 4
Refinement statistics for DHX15.

Resolution range (Å)	45.83–2.00
Completeness (%)	100.0
No. of reflections, working set	50047
No. of reflections, test set	2649
Final R_{cryst} (%)	22.8
Final R_{free} (%)	26.5
No. of non-H atoms	5542
Average *B* factor (Å^2)	62.4
R.m.s. deviations	
Bonds (Å)	0.010
Angles (°)	1.49
Ramachandran plot	
Most favoured (%)	93.9
Allowed (%)	4.2
Disallowed (%)	1.3

Motifs I (also indicated as the P-loop), II, V and VI were engaged in canonical interactions with ADP (Figs. 3*b* and 3*c*). Gly163, Gly165, Lys166, Thr167 and Thr168 (in motif I) were bound to ADP through hydrogen bonds. A magnesium ion and its coordinated water molecules formed a bridge between the β-phosphate of ADP and the surrounding residues of motifs I, II and V. Asp431 (motif V) and Arg475 (motif VI) formed hydrogen bonds to the 2′-OH group of the ribose. The adenine base was stacked between Phe401 and Arg204, which are conserved in all DEAH helicases (Figs. 1 and 3*c*). Similar to other DEAH/RHA proteins, DHX15 lacks the Q-motif, which mediates specific interaction with adenine bases in other helicases such as DEAD-box proteins. Therefore, the adenine base of ADP was not specifically recognized by DHX15 (Fig. 3*c*).

3.3. DHX15 has a positively charged pocket as a potential RNA-binding site

Although it has been shown that both single-stranded (ss) and double-stranded RNAs can act as ligands for DHX15 independent of their sequences (Wang *et al.*, 2015; Lu *et al.*,

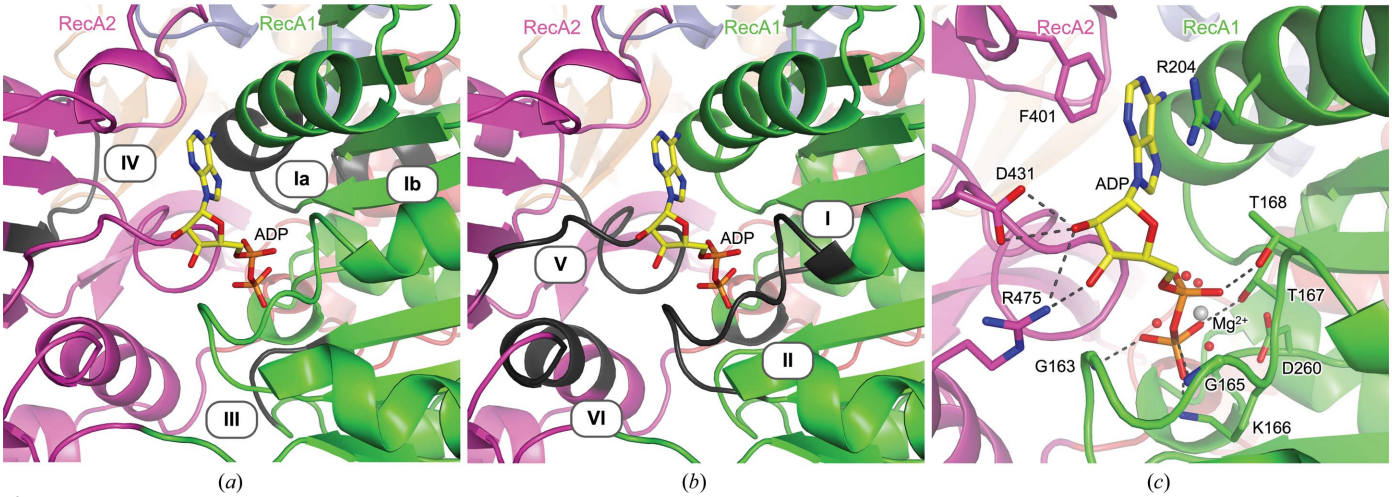

(*a*) (*b*) (*c*)

Figure 3
Structures of sequence motifs of DHX15 conserved in the helicase family. (*a*) Motifs Ia, Ib, III and IV, which are involved in binding to and unwinding of nucleic acid ligands. (*b*) Motifs I, II, V and VI, which are involved in nucleotide recognition. (*c*) ADP recognition by DHX15. The motifs are coloured in black in (*a*) and (*b*). Motifs I–III are located in the RecA1 domain and motifs IV–VI in the RecA2 domain. Polar interactions are indicated by dashed black lines. A magnesium ion and water molecules, which mediate ADP recognition, are shown as a grey sphere and red spheres, respectively.

2014), the precise mechanism by which DHX15 recognizes RNA remains unknown. In general, SF2 helicases bind to nucleic acid ligands using a conserved surface, which contains motifs Ia and Ib in RecA1 and motif IV in RecA2, opposite to the nucleotide-binding site (Fairman-Williams *et al.*, 2010; Leitão *et al.*, 2015; Byrd & Raney, 2012; Jankowsky & Fairman, 2007; Figs. 1 and 2*a*). Interestingly, we found a highly positively charged pocket in DHX15 between the two RecA domains and the CTD (Fig. 4). The entrance to the pocket was formed by the RecA2, ratchet and OB-fold domains. The pocket had an internal diameter of about 10–20 Å and a depth of about 30 Å. The pocket was comprised of many basic residues: Arg194, Arg195, Arg222, Arg243 (RecA1), Arg329, Arg368, Lys443, Lys445, Arg469 (RecA2), Arg504 (WH), Arg602 (ratchet) and Arg748 (OB-fold). The putative RNA-binding motifs of the RecA domains comprised the inner surface of the pocket, along with the CTD (Fig. 4*b*). This suggested that the pocket might be an RNA-binding site.

3.4. Structural comparison between human DHX15 and fungal Prp43

Recent studies have revealed the structure of Prp43, a fungal orthologue of DHX15, in three different states: bound to ADP (scPrp43 and ctPrp43), bound to an ATP analogue (ctPrp43) and bound to an ATP analogue and ssRNA (scPrp43 and ctPrp43) (Tauchert *et al.*, 2016, 2017; Walbott *et al.*, 2010; He *et al.*, 2010). The sequence identities between DHX15 and scPRP43, between DHX15 and ctPrp43, and between scPrp43 and ctPrp43 are 55.7, 54.9 and 65.6%, respectively (Fig. 1).

The compact structure of ADP-bound DHX15 was similar to that of ADP-bound Prp43 in terms of domain structure and organization (Figs. 5*a* and 5*b*). The root-mean-square deviation (r.m.s.d.) values of DHX15 from the ADP-bound form of scPrp43 (PDB entry 2xau; Walbott *et al.*, 2010) and ctPrp43 (PDB entry 5d0u; Tauchert *et al.*, 2016), respectively, were 1.2 and 0.8 Å overall, 0.6 and 0.8 Å for RecA1-RecA2, and 0.8 and 0.7 Å for the CTD for corresponding C^{α} atoms. In contrast, the structure of DHX15 was distinct from that of Prp43 in complex with the ATP analogue and ssRNA, as indicated by the larger r.m.s.d. values of 2.9 and 2.1 Å for scPrp43 (PDB entry 5i8q; Y. He, K. H. Nielsen, G. R. Andersen & J. Staley, unpublished work) and ctPrp43 (PDB entry 5lta; Tauchert *et al.*, 2017), respectively. All of the residues involved in the interaction with ADP were conserved between DHX15 and Prp43, both of which exhibited identical ADP-recognition modes (Figs. 1 and 5*c*).

We identified a positively charged pocket as a potential RNA-binding site in DHX15 (Fig. 4). In the structure of the ADP-bound Prp43, a similar pocket is found between the two RecA domains and the CTD, similar to that in DHX15 (Tauchert *et al.*, 2016, 2017; Walbott *et al.*, 2010; He *et al.*, 2010). Upon binding to the ATP analogue and ssRNA, Prp43 undergoes structural rearrangements of the CTD and the RecA2 domain relative to the RecA1 domain (Tauchert *et al.*, 2017). As a result, in the ssRNA-bound form of Prp43 the pocket splits into a groove, thus accommodating ssRNA (Tauchert *et al.*, 2017). Most of the residues involved in the interaction with ssRNA in ctPrp43 were conserved in DHX15, including Arg194, Arg195, Arg222, Thr237, Arg243, Thr421 and Asn422 (Fig. 1), suggesting that similar structural rearrangements and RNA-recognition mechanisms might exist in human DHX15.

The OB-fold domain plays roles in regulating the helicase activity and RNA-dependent ATPase activity of Prp43/DHX15 through interaction with RNA and G-patch domain-containing proteins (Memet *et al.*, 2017; Walbott *et al.*, 2010; Christian *et al.*, 2014). In previous reports, the regions of the OB-fold domain that are responsible for their interactions

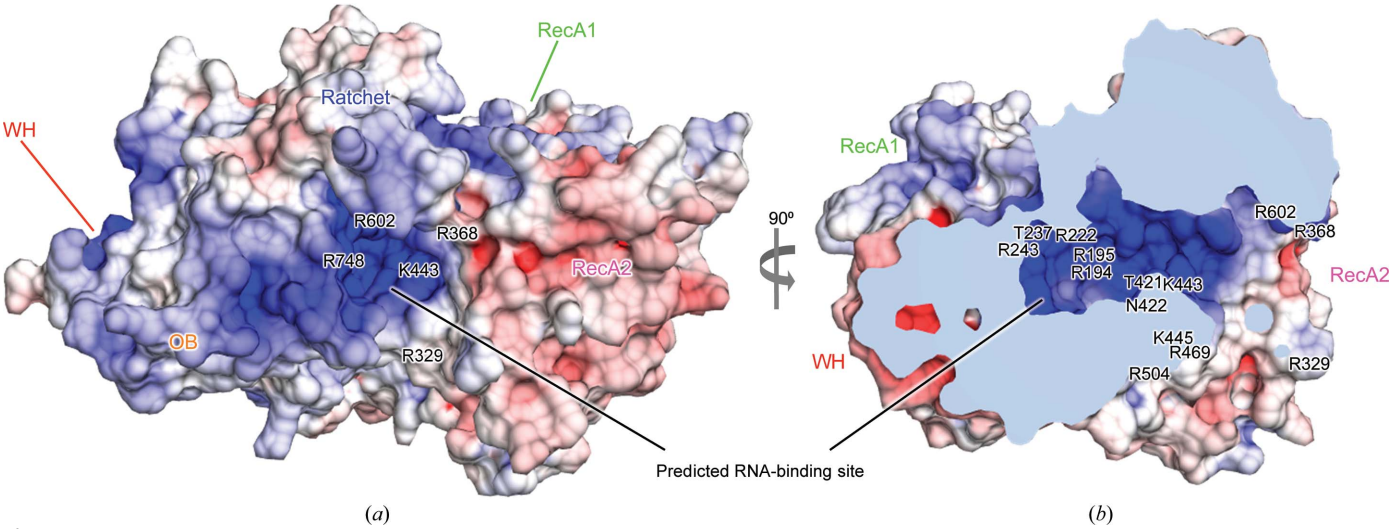

(*a*) (*b*)

Figure 4
Electrostatic surface potential of DHX15. (*a*) The molecular surface of DHX15, showing electrostatic surface potential, viewed from the RecA2 and CTD sides. (*b*) Cutaway surface showing the inner surface of the pocket, viewed from the CTD side. The electrostatic surface potential, calculated using *APBS* (Baker *et al.*, 2001), was visualized with *CueMol* (http://www.cuemol.org). Positively charged and negatively charged surfaces are coloured blue and red, respectively. Some residues are labelled.

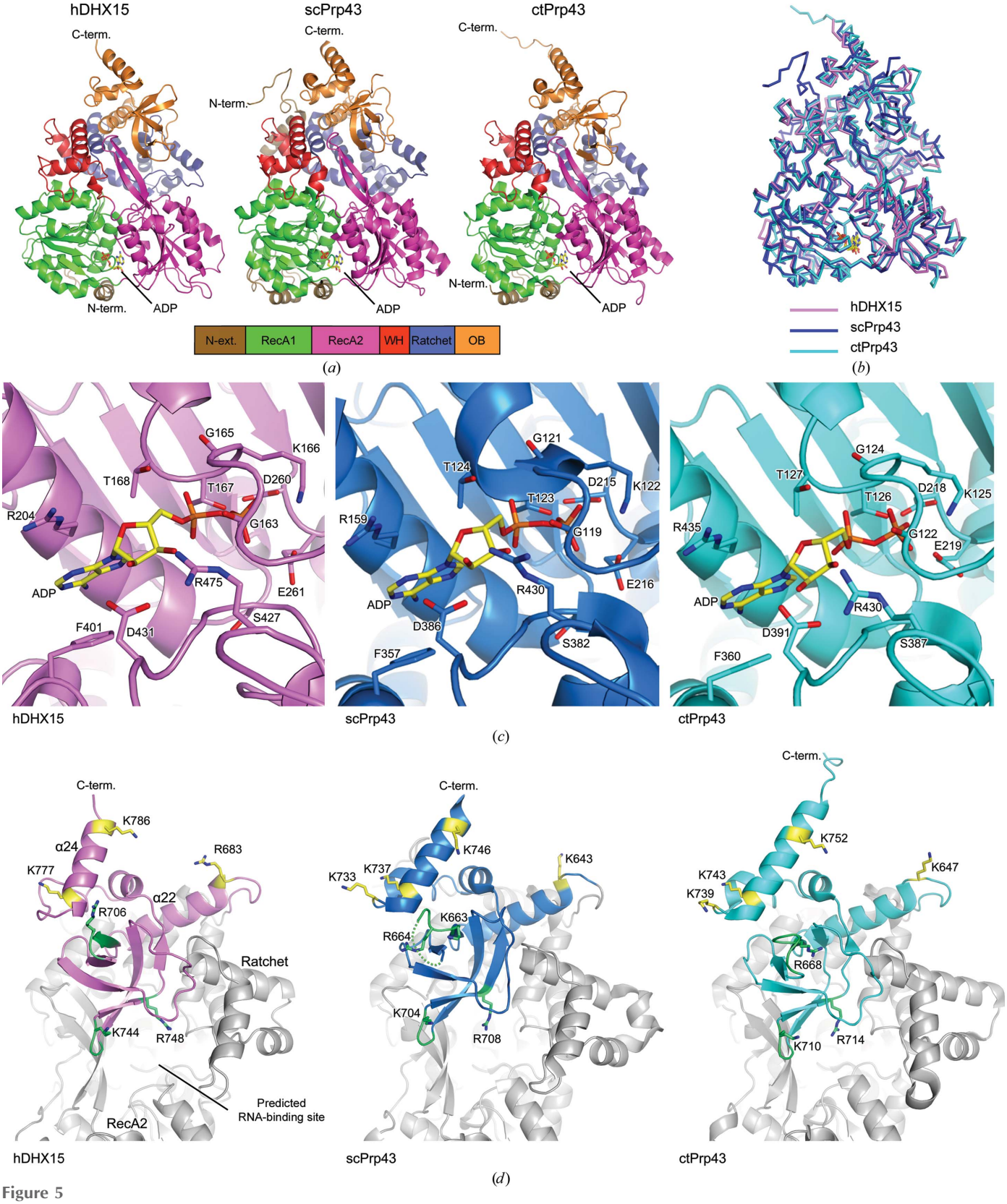

Figure 5

Structural comparison between DHX15 and Prp43. (*a*) Cartoon models of the ADP-bound forms of human DHX15 (hDHX15; this study), scPrp43 (PDB entry 2xau; Walbott *et al.*, 2010) and ctPRP43 (PDB entry 5d0u; Tauchert *et al.*, 2016). (*b*) Superposition of these three structures coloured as follows: hDHX15, violet–pink; scPrp43, blue; ctPrp43, cyan. (*c*) ADP recognition by hDHX15 (left), scPrp43 (middle) and ctPrp43 (right). (*d*) The structures of the OB-fold domains of hDHX15 (violet–pink), scPrp43 (blue) and ctPrp43 (cyan). The residues of scPrp43 that are involved in the interactions with Ntr1 (Christian *et al.*, 2014) and with RNA (Walbott *et al.*, 2010) are coloured yellow and green, respectively. The residues that are implicated in interaction with RNA and the G-patch domain-containing protein Ntr1 in scPrp43 are mostly conserved in hDHX15.

have been studied: residues involved in the interaction between scPrp43 and the G-patch protein Ntr1 are located in α22 and α24 as determined by cross-linking and mass spectrometry (Christian *et al.*, 2014), and the two loop regions located on the both sides of the β-barrel and Arg708 on the inner surface of the potential RNA-binding site play a role in enhancing the RNA-binding and RNA-dependent ATPase activity in scPrp43 (Walbott *et al.*, 2010). Most of these structural elements are conserved among DHX15 and Prp43s (Fig. 5*d*). Therefore, it is likely that the activity of human DHX15 is also regulated by RNA and G-patch domain-containing proteins in the same way as Prp43.

4. Discussion

Although DHX15 is known to be important for both RNA metabolism and innate immune responses to viral RNA, the latter is specific to mammalian DHX15. This study revealed the overall architecture of human DHX15, which was found to be similar to that of its fungal orthologue Prp43, suggesting that the fundamental mechanism in RNA metabolism might be conserved. However, the mechanisms behind the specific mammalian functions of DHX15 remain unknown.

A possible explanation is that mammalian DHX15 has evolved to interact with multiple binding partners that act as effectors for specific functions on different surfaces depending on the proteins. For detecting viral RNA, DHX15 associates with NLRP6, an innate immune receptor (Wang *et al.*, 2015). By analogy to a related system, in which the DEAH/RHA protein DHX33 mediates RNA-induced innate immune responses by interacting with NLRP3 using the RecA1 domain (Mitoma *et al.*, 2013), it is possible that the RecA1 domain of DHX15 is also involved in interaction with NLRP6. On the other hand, DHX15 is known to interact with various G-patch domain-containing proteins *via* the OB-fold domain (Robert-Paganin *et al.*, 2015), and some of these interactions are related to specific mammalian functions of DHX15. For example, DHX15 forms a complex with the G-patch domain-containing protein NKRF and stimulates the 5′–3′ exonuclease XRN2 to process the A′ site in the 5′ external transcribed spacer of ribosomal RNA, a molecular signature specific to metazoans, in the early stages of pre-ribosomal RNA splicing (Memet *et al.*, 2017; Sloan *et al.*, 2014; Henras *et al.*, 2008).

Although the N-terminal extension sequences of DHX15 are highly conserved among mammals, they differ considerably among organisms from different classes (Fig. 1). Thus, their differences may be related to species-specific functions of DHX15. Interestingly, deletion of the first 60 residues of ctPrp43 causes an increased activity in *in vitro* spliceosome disassembly assay in yeast, suggesting its inhibitory role in Prp43 activation (Tauchert *et al.*, 2016). Although the ctPrp43 structure lacks the N-terminal extension owing to truncation to aid crystallization (Tauchert *et al.*, 2016, 2017), the N-terminal extension of scPrp43 forms a long loop structure that simultaneously interacts with the CTD in the N-terminal region and with the RecA1 domain in the C-terminal region (Walbott *et al.*, 2010; He *et al.*, 2010; Fig. 5*a*). These interactions might restrict the structural rearrangement during the activation of DHX15. Similarly, the N-terminal extension of mammalian DHX15, which was deleted in this study and which contains a characteristic repetitive sequence that is rich in charged residues (Arg, Lys, Asp and Glu; Fig. 1), might play specific roles in specific mammalian functions of DHX15. However, further studies are required to define the roles of this region.

Many questions remain unanswered regarding the mammalian DEAH/RHA proteins. Although many reports have been published on the structures of fungal orthologues, partly because of the lack of structural information available the structure, functions and mechanisms of mammalian DEAH/RHA proteins remain largely unknown. In this study, the first structure of a mammalian DEAH/RHA protein containing almost all of the domains has been reported. This information will be useful not only to study the activation mechanism of DHX15 in humans, but also to further our understanding of mammalian DEAH/RHA proteins, which are important for many biological processes such as splicing and innate immune sensing.

Acknowledgements

We thank Drs Y. Yamada and A. Shinoda for automated data collection of the initial data set at Photon Factory. This work was supported by a Grant-in-Aid from the Japanese Ministry of Education, Culture, Sports, Science and Technology (UO and TS), the Takeda Science Foundation (UO and TS), the Mochida Memorial Foundation for Medical and Pharmaceutical Research (UO), the Daiichi Sankyo Foundation of Life Science (UO) and the Naito Foundation (UO). We declare that none of the authors have financial interests related to this work.

References

Abdelhaleem, M., Maltais, L. & Wain, H. (2003). *Genomics*, **81**, 618–622.
Baker, N. A., Sept, D., Joseph, S., Holst, M. J. & McCammon, J. A. (2001). *Proc. Natl Acad. Sci. USA*, **98**, 10037–10041.
Bohnsack, M. T., Martin, R., Granneman, S., Ruprecht, M., Schleiff, E. & Tollervey, D. (2009). *Mol. Cell*, **36**, 583–592.
Büttner, K., Nehring, S. & Hopfner, K.-P. (2007). *Nature Struct. Mol. Biol.* **14**, 647–652.
Byrd, A. K. & Raney, K. D. (2012). *Front. Biosci.* **17**, 2070.
Chen, V. B., Arendall, W. B., Headd, J. J., Keedy, D. A., Immormino, R. M., Kapral, G. J., Murray, L. W., Richardson, J. S. & Richardson, D. C. (2010). *Acta Cryst.* D**66**, 12–21.
Chen, Y.-L., Capeyrou, R., Humbert, O., Mouffok, S., Kadri, Y. A., Lebaron, S., Henras, A. K. & Henry, Y. (2014). *Nucleic Acids Res.* **42**, 7330–7345.
Christian, H., Hofele, R. V., Urlaub, H. & Ficner, R. (2014). *Nucleic Acids Res.* **42**, 1162–1179.
Combs, D. J., Nagel, R. J., Ares, M. & Stevens, S. W. (2006). *Mol. Cell. Biol.* **26**, 523–534.
DeLano, W. L. (2008). *PyMOL*. http://www.pymol.org.
Emsley, P., Lohkamp, B., Scott, W. G. & Cowtan, K. (2010). *Acta Cryst.* D**66**, 486–501.
Fairman-Williams, M. E., Guenther, U. P. & Jankowsky, E. (2010). *Curr. Opin. Struct. Biol.* **20**, 313–324.

Fourmann, J.-B., Schmitzová, J., Christian, H., Urlaub, H., Ficner, R., Boon, K. L., Fabrizio, P. & Lührmann, R. (2013). *Genes Dev.* **27**, 413–428.
Fu, Q. & Yuan, Y. A. (2013). *Nucleic Acids Res.* **41**, 3457–3470.
He, Y., Andersen, G. R. & Nielsen, K. H. (2010). *EMBO Rep.* **11**, 180–186.
Henras, A. K., Soudet, J., Gérus, M., Lebaron, S., Caizergues-Ferrer, M., Mougin, A. & Henry, Y. (2008). *Cell. Mol. Life Sci.* **65**, 2334–2359.
Imamura, O., Sugawara, M. & Furuichi, Y. (1997). *Biochem. Biophys. Res. Commun.* **240**, 335–340.
Jankowsky, E. & Fairman, M. E. (2007). *Curr. Opin. Struct. Biol.* **17**, 316–324.
Kabsch, W. (2010). *Acta Cryst.* D**66**, 125–132.
Kudlinzki, D., Schmitt, A., Christian, H. & Ficner, R. (2012). *Biol. Chem.* **393**, 1131–1140.
Lebaron, S., Froment, C., Fromont-Racine, M., Rain, J.-C., Monsarrat, B., Caizergues-Ferrer, M. & Henry, Y. (2005). *Mol. Cell. Biol.* **25**, 9269–9282.
Lebaron, S., Papin, C., Capeyrou, R., Chen, Y. L., Froment, C., Monsarrat, B., Caizergues-Ferrer, M., Grigoriev, M. & Henry, Y. (2009). *EMBO J.* **28**, 3808–3819.
Leeds, N. B., Small, E. C., Hiley, S. L., Hughes, T. R. & Staley, J. P. (2006). *Mol. Cell. Biol.* **26**, 513–522.
Leitão, A. L., Costa, M. C. & Enguita, F. J. (2015). *Int. J. Mol. Sci.* **16**, 2269–2293.
Liu, Y., Lu, N., Yuan, B., Weng, L., Wang, F., Liu, Y.-J. & Zhang, Z. (2014). *Cell. Mol. Immunol.* **11**, 49–57.
Lu, H., Lu, N., Weng, L., Yuan, B., Liu, Y. & Zhang, Z. (2014). *J. Immunol.* **193**, 1364–1372.
Memet, I., Doebele, C., Sloan, K. E. & Bohnsack, M. T. (2017). *Nucleic Acids Res.* **45**, 5359–5374.
Mitoma, H., Hanabuchi, S., Kim, T., Bao, M., Zhang, Z., Sugimoto, N. & Liu, Y.-J. (2013). *Immunity*, **39**, 123–135.
Miyashita, M., Oshiumi, H., Matsumoto, M. & Seya, T. (2011). *Mol. Cell. Biol.* **31**, 3802–3819.
Murshudov, G. N., Skubák, P., Lebedev, A. A., Pannu, N. S., Steiner, R. A., Nicholls, R. A., Winn, M. D., Long, F. & Vagin, A. A. (2011). *Acta Cryst.* D**67**, 355–367.
Myong, S., Cui, S., Cornish, P. V., Kirchhofer, A., Gack, M. U., Jung, J. U., Hopfner, K.-P. & Ha, T. (2009). *Science*, **323**, 1070–1074.
Niu, Z., Jin, W., Zhang, L. & Li, X. (2012). *FEBS Lett.* **586**, 977–983.
Oshiumi, H., Sakai, K., Matsumoto, M. & Seya, T. (2010). *Eur. J. Immunol.* **40**, 940–948.
Pertschy, B., Schneider, C., Gnädig, M., Schäfer, T., Tollervey, D. & Hurt, E. (2009). *J. Biol. Chem.* **284**, 35079–35091.
Robert, X. & Gouet, P. (2014). *Nucleic Acids Res.* **42**, W320–W324.
Robert-Paganin, J., Réty, S. & Leulliot, N. (2015). *Biomed. Res. Int.* **2015**, 931857.
Singleton, M. R., Dillingham, M. S. & Wigley, D. B. (2007). *Annu. Rev. Biochem.* **76**, 23–50.
Sloan, K. E., Bohnsack, M. T., Schneider, C. & Watkins, N. J. (2014). *RNA*, **20**, 540–550.
Tanaka, N. & Schwer, B. (2006). *Biochemistry*, **45**, 6510–6521.
Tannukit, S., Crabb, T. L., Hertel, K. J., Wen, X., Jans, D. A. & Paine, M. L. (2009). *Biochem. Biophys. Res. Commun.* **390**, 1044–1050.
Tauchert, M. J., Fourmann, J.-B., Luhrmann, R. & Ficner, R. (2017). *Elife*, **6**, e21510.
Tauchert, M. J., Fourmann, J.-B., Christian, H., Lührmann, R. & Ficner, R. (2016). *Acta Cryst.* F**72**, 112–120.
Vagin, A. & Teplyakov, A. (2010). *Acta Cryst.* D**66**, 22–25.
Walbott, H., Mouffok, S., Capeyrou, R., Lebaron, S., Humbert, O., van Tilbeurgh, H., Henry, Y. & Leulliot, N. (2010). *EMBO J.* **29**, 2194–2204.
Wang, P., Zhu, S., Yang, L., Cui, S., Pan, W., Jackson, R., Zheng, Y., Rongvaux, A., Sun, Q., Yang, G., Gao, S., Lin, R., You, F., Flavell, R. & Fikrig, E. (2015). *Science*, **350**, 826–830.
Zhang, Z., Kim, T., Bao, M., Facchinetti, V., Jung, S. Y., Ghaffari, A. A., Qin, J., Cheng, G. & Liu, Y.-J. (2011). *Immunity*, **34**, 866–878.
Zhang, Z., Yuan, B., Lu, N., Facchinetti, V. & Liu, Y.-J. (2011). *J. Immunol.* **187**, 4501–4508.